Design and Estimation of the Accuracy Parameters of a Digital Surface Model (DSM) Using a DJI Phantom 4 Pro Drone and Photogrammetry Technique

Pinatibi, H.,* Ouattara, G. J. and Edi, K. H.
Department of Fundamental Applied Sciences, Mathematics and Computer Science Laboratory,
Nangui Abrogoua University, Côte d'Ivoire, 01 PO Box 802 Abidjan 01
E-mail: pinatibih@gmail.com,* gnjustin.ic@gmail.com, edi.hilaire@gmail.com
**Corresponding Author*

DOI: https://doi.org/10.52939/ijg.v20i11.3681

Abstract
A Digital Surface Model (DSM) represents terrain elevation, incorporating natural and artificial features within an environment. These models are valuable in fields like telecommunications for analyzing electromagnetic wave propagation. However, DSMs are approximations due to errors from acquisition tools, data collection conditions, and processing methods. This study presents a methodology for producing a DSM and calculating its accuracy using a DJI Phantom 4 Pro drone at altitudes of 30 m, 50 m, and 70 m. Images captured were processed with photogrammetry techniques using Pix4Dmapper software. For the respective altitudes, 374, 154, and 80 images were collected at a resolution of 5472×3648 pixels. The photogrammetry technique, employing the Triangulated Irregular Network (TIN) interpolation method, achieved optimal accuracies during the 30 m flight, with planimetric accuracies of 13 cm in the East-West direction and 17 cm in the North-South direction, and distance and height accuracies of 12 cm and 15 cm. This study demonstrates that high planimetric precision and accurate ground structure representation are achievable using drone-based DSM generation.

Keywords: Drone, DSM, Photogrammetry, RMSE, UA

1. Introduction

A Digital Surface Model (DSM) is a representation of terrain relief and visible elements on the ground, including buildings, vegetation, and other features. It is a technique for the digital representation of an environment that relies on mathematical formulas to determine the altitude of any point on the Earth's surface within a well-defined reference system [1] and [2]. DSMs are extensively utilized in various fields, such as geomorphology for studying geological structures, hydrology for identifying water flow areas, telecommunications for analyzing electromagnetic wave propagation, and cartography and security services, among others [3].

The advantages of DSMs are undeniable [4]. In advanced applications, particularly in telecommunications, detailed environmental modeling is essential to accurately study electromagnetic wave propagation. Hence, thoroughly characterizing the environment with all its possible forms becomes crucial to minimize errors in the final results [5] and [6].

While DSMs provide a highly accurate representation of an environment, they remain approximations of reality [7]. Errors can arise during data acquisition due to meteorological conditions or the performance limitations of the acquisition tools used. Additionally, transitioning between different processing software can introduce further errors [8]. Consequently, many researchers emphasize the importance of studying and estimating these errors in digital terrain representations [3].

Organizations like OpenStreetMap (OSM) and the World Meteorological Organization (WMO) are dedicated to producing these models using advanced data acquisition tools, which are often costly. However, it is also possible to create DSMs using more accessible means, depending on the specific needs. This can involve using Unmanned Aerial Systems (UAS), particularly drones, in aerial photogrammetry a technique that enables the collection of precise geographic data from images captured by aerial platforms [9] and [10].

Depending on the requirements and available resources, tools are adapted to prioritize either the size of the study area or the quality of data, especially regarding altimetric and planimetric accuracy.

The aerial photogrammetry process begins with capturing stereoscopic aerial images from a flying platform. These images are taken from different positions and angles to ensure comprehensive coverage of the area of interest. Once captured, the images undergo a restitution process to extract geometric information from the features. This process, known as photogrammetry, relies on advanced mathematical and algorithmic principles. Photogrammetry software employs techniques such as image correlation, triangulation, image block adjustment, and stereoscopy to compute three-dimensional coordinates of points of interest in space. The outputs of aerial photogrammetry can be represented as point clouds, digital terrain models (DTM), or digital surface models (DSM) [1].

In aerial photogrammetry, several techniques are available for acquiring altimetric data, including satellite-based methods, aircraft, drones, and other flying objects [11]. For extensive areas on a continental or even global scale, satellites are preferred for image acquisition due to their ability to cover large regions efficiently. The data obtained through satellite methods are primarily utilized to construct Digital Elevation Models (DEMs). When dealing with a country or regional scale, aircraft equipped with high-definition cameras are the most suitable tools for data collection. Some researchers argue that these two techniques satellite and aircraft are particularly well-suited for acquiring high-density altimetric data (several points per square meter) over medium to large areas [1]. However, these methods often fall short in accurately capturing the true shapes of features such as buildings and trees.

A more appropriate tool for generating DSMs is the use of drones, as they operate closer to the ground and can capture high-resolution images from varying angles [12]. Previous studies have shown that the accuracy of altimetric data obtained from low-altitude aerial photography using drones can range from 2 cm to 20 cm on flat, sandy terrain, with a flight altitude of approximately 153 meters [13]. Thus, drones enable centimeter-level accuracy and provide detailed observations of the environment's shape and texture. This article examines the methodology for producing a high spatial resolution DSM using accessible tools and also aims to identify and analyze its accuracy parameters. It is important to note that the study area includes various features such as buildings and trees, which will be modeled. The primary objective is to create a DSM with high planimetric accuracy that can accurately represent the dimensions (length, width, and height) of each ground structure (referred to as distance and height accuracy in this document), including buildings and trees. The focus will be on using drones to capture more detailed environmental data and applying photogrammetry techniques for DSM generation. The resulting model will be utilized to extract the height of each structure (building and tree) on the ground, which provides crucial data for applications in fields such as telecommunications. As DSMs are not free from errors, this study will also present existing methods for describing errors by comparing real-world data with those obtained from the DSM.

2. Materials and Methods

2.1 Materials

2.1.1 Drone

To generate the Digital Surface Model (DSM), a DJI Phantom 4 Pro drone equipped with an integrated camera was utilized. The specifications of both the drone and its camera are detailed in Table 1. The DJI Phantom 4 Pro drone was selected for this study due to its cost-effectiveness (approximately 496.38 USD) and its capability to collect high-resolution imagery. The drone provides optimal stability during flight, minimizing the impact of wind disturbances, which is crucial for capturing precise data. Additionally, it is equipped with an obstacle avoidance system, enhancing ease of use even for users with limited experience in drone operation. The integrated camera on the DJI Phantom 4 Pro is of high quality, capable of capturing images at a resolution of up to 5472×3648 pixels (around 20 million pixels per image). This level of resolution is more than adequate for obtaining reliable results after photogrammetric processing. Moreover, the camera is multispectral, meaning it can capture images across various wavelengths. This feature allows for the differentiation of material types, the measurement of surface reflectivity, and more accurate reconstruction of environmental shapes and structures. The DJI Phantom 4 Pro, with its combination of advanced features, is well-suited for accurate 3D modeling and is thus ideal for generating a precise Digital Surface Model (DSM) in this study.

2.1.2 Phone

To operate the drone, a compatible smartphone with the appropriate flight software is required. For this study, an Infinix HOT 8 smartphone was selected due to its compatibility with the DJI GO software. The specifications of the Infinix HOT 8 are provided in Table 2.

Table 1: Specifications of the DJI drone and its integrated camera

DJI Phantom 4 Pro Drone	
Weight (battery and propellers included)	1388g
Diagonal size (propellers excluded)	350 mm
Maximum flight time	30 mn
Max Wind speed resistance	10m/s
Satellite positioning systems	GPS/GLONASS
Hover accuracy range	*Vertical*: +/- 0.1 m (when the visual positioning system is activated) or +/- 0.5 m *Horizontal*: +/- 0.3 m (when visual positioning system is activated) or +/- 1.5 m

Built-in camera features	
Sensor	CMOS 1'' Effective pixels: 20 M (20 megapixels)
Objective	FOV 84° 8.8 mm/24 mm (35 mm format equivalent) f/2.8 - f/11 autofocus at 1 m - ∞
ISO range	Video: 100 - 3200 (Auto) 100 - 6400 (Manual) Photo: 100 - 3200 (Auto) 100-12800 (Manual)
Pictures's size	Aspect ratio: 3:2; Aspect ratio: 5472×3648 px Format: 4:3; Aspect ratio: 4864×3648 px Aspect ratio: 16:9; Aspect ratio: 5472×3078 px

Table 2: Phone specifications

Description	Specification
Name	Infinix HOT 8
Model	Infinix X650B
Android version	9
RAM	2 GB
ROM	32 GB

2.1.3 Computer

To process the collected images effectively, it is crucial to use a high-performance computer. The large size of the data and the complexity of the algorithms used in photogrammetry require substantial computational resources. For instance, PIX4Dmapper software, which is used in this study, recommends a computer with a minimum of 16 GB of RAM to handle the processing tasks efficiently. For this study, an HP computer with a high-performance graphics card was used to successfully process the photogrammetry data. The specifications of this computer are detailed in Table 3.

2.2 Methods

2.2.1 Data collection

The data collection phase involved capturing photographs of the area of interest while carefully considering several parameters and conditions to ensure accurate 3D model reconstruction. Each photo's metadata included the geographic coordinates of the capture point, the camera's tilt angle, and other relevant information. The photographs were taken under clear and uniform sky conditions, with wind speeds kept below 10 m/s, as indicated by the flight day's meteorological data, to ensure drone stability [14] [15] and [16]. The data collection process is summarized in 4 points which are: choice of flight planning software, flight planning on 3Dsurvey Pilot (in our case), drone-phone connection and taking photos (Figure 1).

Table 3: Computer specifications

Description	Specification
CPU	Intel(R) Core (TM) i7- 10700 CPU@2.90 GHz
RAM	32 GB
GPU	NVIDIA GeForce GTX 1660, Intel(R) UHD Graphics 630
OS	Windows 10 Pro, 64-bit

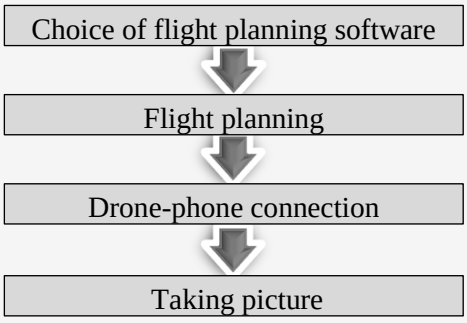

Figure 1: Data collection process

• *Choice of Flight Planning Software*

A variety of online software platforms are available for planning intelligent flights aimed at collecting altimetric data, including options such as DroneDeploy, Pix4Dcapture, and 3Dsurvey Pilot. These tools enable the definition of coverage areas, the determination of optimal flight paths, and the generation of automated flight plans that ensure comprehensive image capture with the appropriate overlap. In this study, 3Dsurvey Pilot was selected due to several key factors, including software compatibility and cost. Not all applications are universally compatible with every smartphone; for example, DroneDeploy is incompatible with the Infinix Hot 8 X650B model. After confirming software compatibility with the device, it is essential to evaluate usage costs. For initial testing, a cost-effective solution is preferable. 3Dsurvey Pilot was identified as the optimal choice, offering compatibility with the selected phone, ease of configuration, straightforward connection with the drone, and useful features available at no cost in its standard version.

• *Flight Planning on 3Dsurvey Pilot*

The 3Dsurvey Pilot app, in its trial version, provides various free flight options, including 2D or 3D grid flights, circle flights, polygon flights, and more. Circular flights are typically used for projects focusing on a specific element, such as a building or a telecommunications antenna. Given that the study area in this work contains multiple buildings and trees, a double grid flight pattern was selected to ensure comprehensive coverage. After selecting the flight type, the app presents an intuitive interface with several configurable parameters. The first step involves defining the area to be covered on the geographical map. In this study, the area includes the building complex of the Institute for New Energy Research (IREN), the vice-presidency of Nangui Abrogoua University, and the surrounding environment. A default lateral overlap of 70% for images was maintained to ensure adequate coverage.

A drone speed of 4 m/s was selected to prevent blurred images, a critical requirement for this project conducted in a complex area that requires high accuracy in the resulting photogrammetric data (DSM). Additionally, this speed optimizes the time needed for image collection, ensuring complete coverage of the study area in a single flight, thereby balancing the need for quality with operational efficiency. The camera was oriented from the front of the drone downwards, with a tilt angle of 75°, allowing for clear capture of building facades. The drone's takeoff point was set as the 0 m altitude mark, ensuring that only the heights of the ground structures were recorded. The complete configuration details are summarized in Table 4.

• *Drone-Phone Connection*

The connection process between the drone and the phone involves several key steps. First, the phone containing the flight plan must be connected to the drone. A memory card with a minimum capacity of 64 GB should then be inserted into the drone. Next, the phone is connected to the drone's remote control using a USB cable. The DJI GO app is then launched on the phone, followed by minimizing the app and

opening the 3Dsurvey Pilot app. It is important to wait until all indicators in the app turn green, indicating that the system is ready, before initiating the flight by pressing the "Start" button. Care must be taken to ensure that the drone is not placed on a metallic surface, as this could disrupt the connection to the satellites and affect the accuracy of the flight plan.

- *Taking Pictures*

Once all conditions were met, all indicators turned green, and the "Start" button became active. By simply clicking this button to initiate the mission, the drone automatically took off, ascended to the programmed altitude, captured all necessary images, and returned to the starting point. Figure 2 shows the study area, which is Nangui Abrogoua Universit and the six GCPs collected.

2.2.2 Data Processing using Photogrammetry

In this study, Pix4Dmapper software was utilized to apply the photogrammetry process to the collected data. The photogrammetry workflow in Pix4Dmapper comprises six steps (Figure 3). The first step (1) involves creating a new project and loading the images into the software, each image being loaded with its geographic coordinates, although it is possible to modify them.

Table 4: Flight configuration and planning

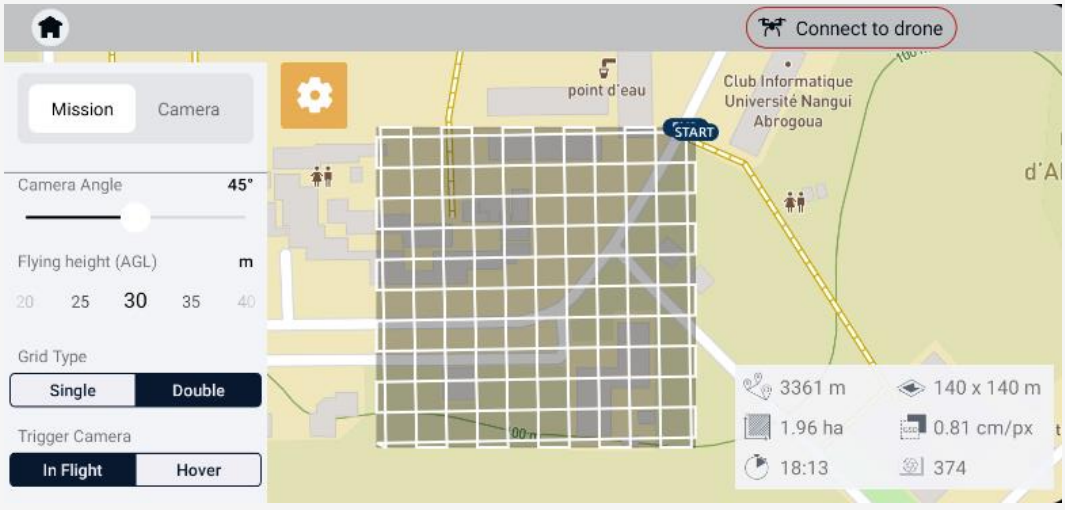

Date	Flight 1 : 26-09-2023	Flight 2 : 27-09-2023	Flight 3 : 02-10-2023
Skies status according the day's weather	Clear skies, fully sunny	Skies not very clear, with constant brightness	Clear skies, sunny with constant brightness
Wind speed according the day's weather (km/h)	Around 16	Around 15	Around 18
Lateral overlap	70%	70%	70%
Maximum speed	4m/s	4m/s	4m/s
Camera tilt angle	75°	75°	75°
Flight height (above ground)	30 m	50 m	70 m
Area	140m²	140m²	140m²
Duration of planned flight	18mn 13s	12mn 20s	9mn 10s
Expected number of pictures	374	154	80
Take-off point	5.388084, -4.017763	5.388084, -4.017763	5.388084, -4.017763

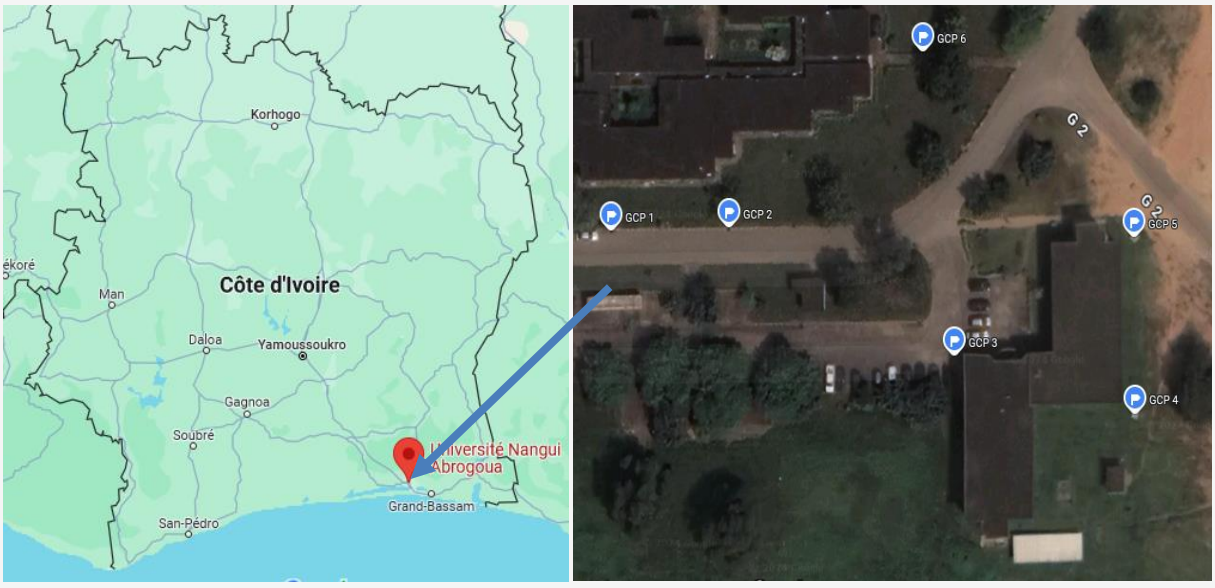

Figure 2: The study area in Nangui Abrogoua University and GCPs

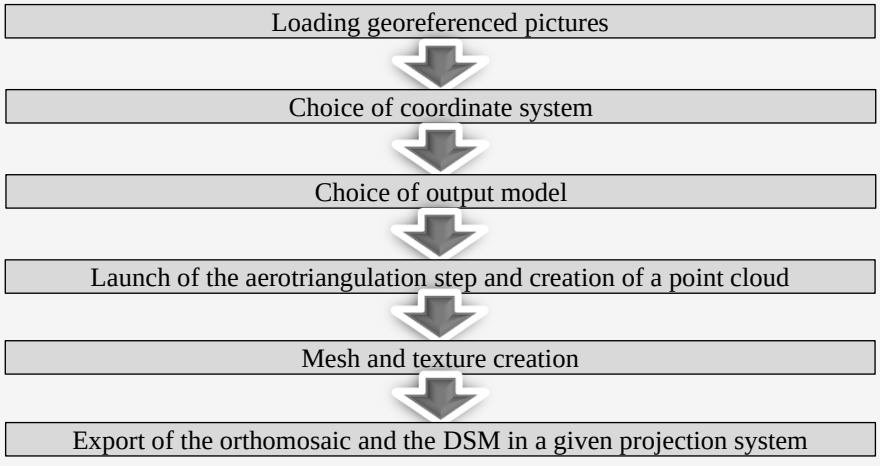

Figure 3: Photogrammetry data processing

Next (2), the coordinate system to be used in the process is selected. By default, Pix4Dmapper chooses the World Geodetic System (WGS 84 / UTM zone 30N (EGM 96 Geoid)), which corresponds to the projection system for the study area. In step (3), the output model is selected, and the process is initiated. Step (4) involves aerotriangulation and the creation of a point cloud, where the objective is to reconstruct three-dimensional information from the aerial images. This step focuses on identifying the parameters related to the relative and absolute geometry of the camera used to capture the images, as well as determining the precise spatial coordinates of the points of interest on the ground.

At the end of this step, a three-dimensional point cloud is generated. Given that this point cloud is isolated, a mesh and a texture are created to produce a complete and realistic 3D model using the TIN (Triangulated Irregular Network) interpolation method. Steps (1) through (3) serve to configure Pix4Dmapper before starting the process. In steps (4) and (5), photogrammetry algorithms, such as stereorestitution and triangulation, are employed to refine the 3D model. Step (6) involves exporting the results into different file formats that can be used by Geographic Information System (GIS) software, such as QGIS, ArcGIS, etc.

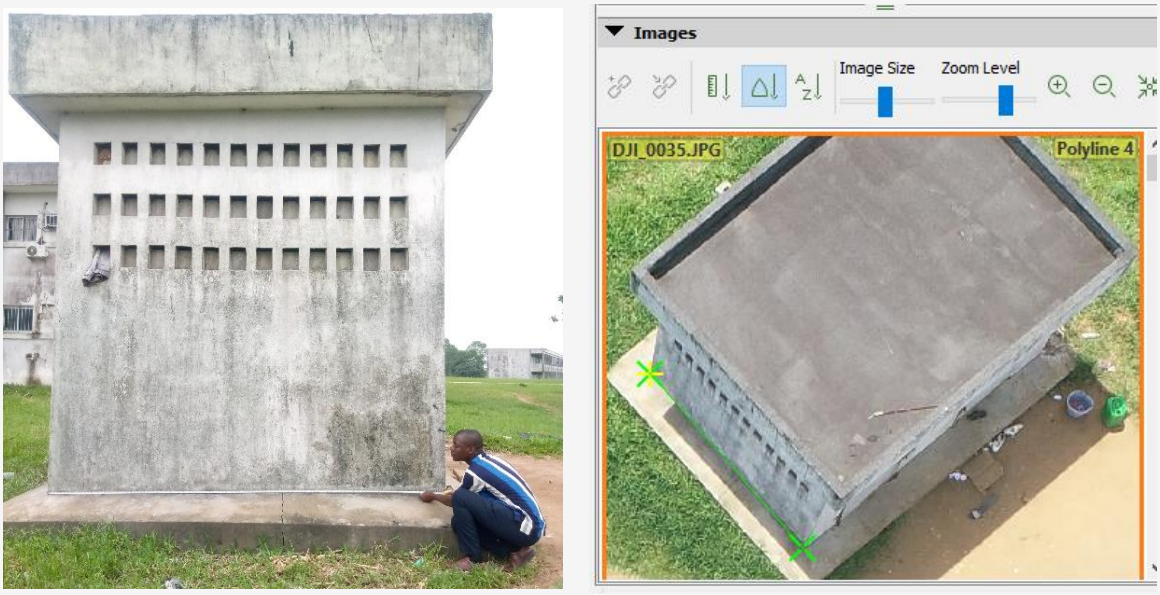

(a) (b)

Figure 4: Horizontal measurement (a) on the ground and (b) on the DSM

(a) (b)

Figure 5: Vertical measurement (a) on the ground (b) on the DSM

2.2.3 Measurements process

Following the photogrammetry processing, the Pix4Dmapper software facilitates the placement of markers on the generated 3D model, enabling the measurement of distances between these markers in both horizontal and vertical directions. To validate these distances in reality, the locations of the markers were replicated on the ground, and a steel measuring tape was utilized to measure the actual distances. Figure 4 provides an example of a horizontal distance measurement between two selected markers, illustrating (a) the actual measurement taken on-site and (b) the corresponding measurement on the DSM. Similarly, Figure 5 presents an example of a height measurement between two points, representing the vertical direction, with (a) showing the actual measurement and (b) depicting the measurement on the DSM.

2.2.4 Accuracy calculation

The DSM generated is not without errors, as flight conditions and the materials used can introduce inaccuracies into the final result. Upon completion of data processing, the Pix4Dmapper software generates a comprehensive quality report detailing the outcomes. Within the geolocation details section of this report, information concerning errors related to geographic coordinates is provided. A critical parameter for error calculation included in the report is the Root Mean Square Error (RMSE).

It is important to note that an error is defined as the difference between a computed value on the DSM and the corresponding actual value recorded on the ground [3]. The RMSE, therefore, quantifies the extent to which the model deviates from the actual measured values by calculating the Euclidean distance. The formula for RMSE used to compute the accuracy in the vertical direction is:

$$RMSE = \sqrt{\frac{\sum_{i=1}^{n} (He_{DSM} - He_{PC})^2}{n}}$$

Equation 1

Where:

He_{DSM} : Height measured on the DSM
He_{PC} : Height measured on the ground
n : Total number of the measurements

To further assess the potential errors, the accuracy of the building length (denoted as *RMS**) was evaluated to verify if a measured distance between two points on the DSM accurately reflects the actual distance on the ground. To accomplish this, ten real-world distances were measured, and their corresponding values were identified on the DSM as illustrated in Figure 4. In this context, the following formula was applied:

$$RMS^* = \sqrt{\frac{\sum_{i=1}^{n} (D_{DSM} - D_{PC})^2}{n}}$$

Equation 2

Where:

D_{DSM} : Distance measured on the DSM
D_{PC} : Actual distance measured on the ground
n : Total number of the measurements

3. Results

3.1 Collection of Data

A total of three flight missions were conducted at varying altitudes: one at 30 meters, another at 50 meters, and the last at 70 meters, with respective flight durations of 18 minutes 13 seconds, 12 minutes 20 seconds, and 9 minutes 10 seconds. During the first mission, 374 pictures were captured; 154 pictures were taken during the second mission, and 80 pictures were captured at the 70-meter altitude. All images captured by the drone were in JPG format, with an approximate file size of 7 MB per image and dimensions of 5472×3648 pixels. Each picture was tagged with the geographic information of the drone at the time of capture, including geographical coordinates and the camera's rotation angles around the X, Y, and Z axes. Common information for all images is summarized in Table 5.

3.2 Treatment by Photogrammetry

After processing each dataset through photogrammetry, the overlap of the captured images from the drone during the first flight was analyzed (Figure 6(a)). The red areas in Figure 6(a) indicate regions covered by only one image during the mission, while the green points represent areas captured in more than five images. This overlap is crucial for ensuring sufficient data coverage, which is why at least a 3-meter margin around the target area is recommended. The corresponding orthophoto generated from the first mission is presented in Figure 6(b). These orthophotos from each mission are exportable and compatible with most GIS software, such as QGIS and ArcGIS. Figure 7 illustrates the Digital Surface Models (DSM) generated from each mission: Figure 7(a) corresponds to the DSM from the first mission at a 30-meter flight height, Figure 7(b) to the DSM from the second mission at a 50-meter height, and Figure 7(c) to the DSM from the third mission at a 70-meter height. In these DSMs, red areas represent the tallest structures, such as buildings and trees, with heights approximately 13.22 meters in Figure 7(a), 13.51 meters in Figure 7(b), and 20.25 meters in Figure 7(c). The blue area indicates the lowest elevation, with height as low as -7.32 meters in Figure 7 and -11.91 meters in Figure 8, relative to the drone's take-off point; this is a swale.

Table 5: Pictures metadata range

Characteristics	H30		H50		H70	
	Min	Max	Min	Max	Min	Max
The rotation angle around the X axis (omega) (°)	-47.93	47.70	-47.55	-48.94	-48.78	47.59
The rotation angle around the Y axis (Phi) (°)	-45.00	47.24	-45.11	-46.38	-45.03	47.64
The rotation angle around the Z axis (Kappa) (°)	-173.53	170.75	-171.52	-178.65	-135.14	168.28
Number of pictures collected	374		154		80	
Processing time	2h 13min		47min		33 min	

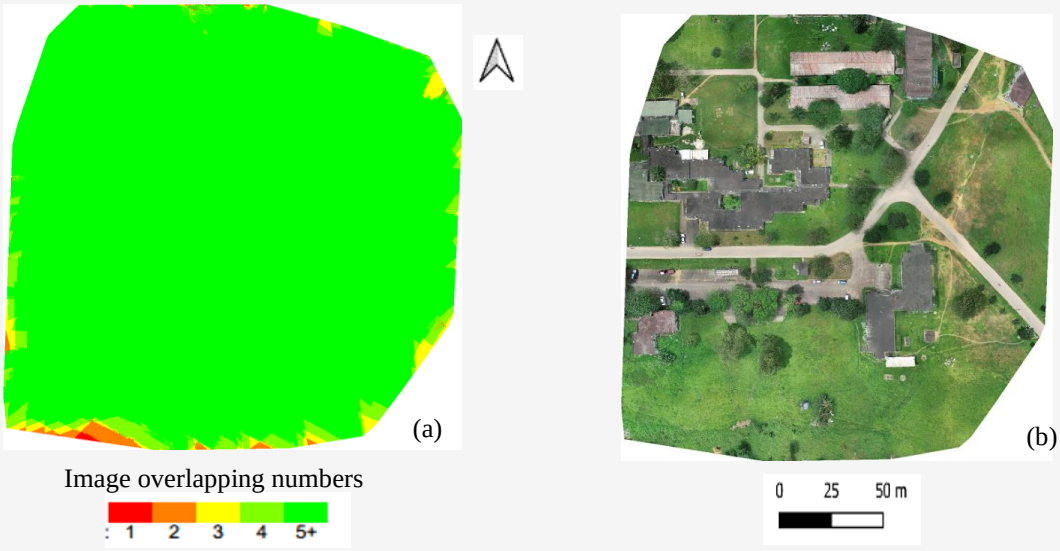

Figure 6: H30 (a)number of overlapping images and (b) orthophoto

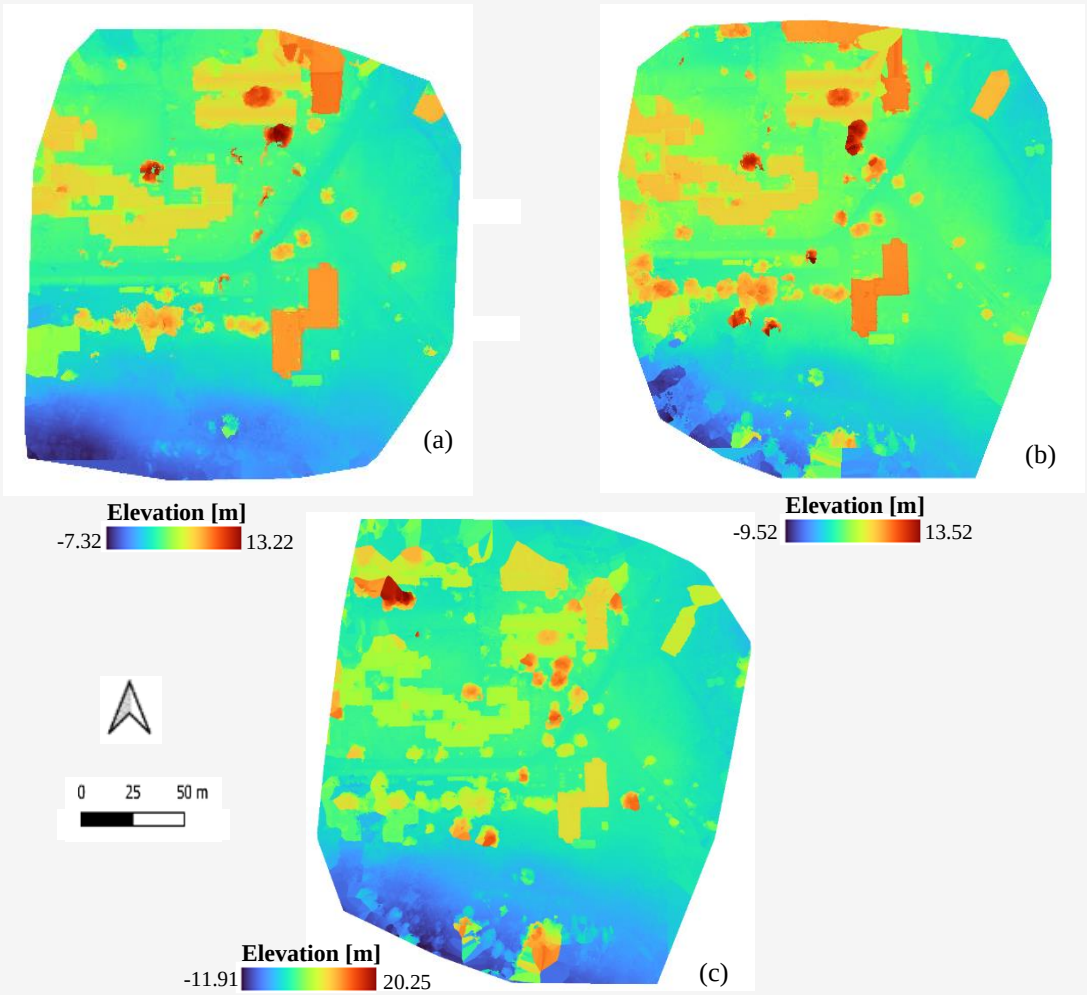

Figure 7: Digital surface model (a) H30, (b) H50 (c) H70

3.3 Planimetric Accuracy

During this study, six Ground Control Points (GCPs) were collected and converted to UTM using objects that were clearly visible in the Digital Surface Models (DSMs), such as slabs and sewer grates (Figure 2). These points were critical for analyzing the planimetric accuracy of the generated DSMs. The analysis revealed that the planimetric precision is within a range of centimeters for flights conducted at an altitude of 30 meters. However, this precision tends to decrease as the flight height increases. Moreover, the accuracy calculated using the differences between the GCP and DSM of Table 6 was found to be higher in the X direction (East-West) compared to the Y direction (North-South), as presented in Table 7.

3.4 Measurement Error

3.4.1 Distance measurement error

Table 8 presents the ten real horizontal distances measured on the ground, their corresponding values on each of the Digital Surface Models (DSMs), and the differences between these values and the estimated values for each of the three missions.

Table 6: Differences between the GCPs and DSMs collected

GCP		GCPs (m)	H30		H50		H70	
			DSM value (m)	Error (m)	DSM value (m)	Error (m)	DSM value (m)	Error (m)
GCP 1	X	387157.69	387157.79	-0.10	387158.25	-0.56	387156.71	0.98
	Y	595667.68	595667.52	0.16	595668.50	-0.82	595666.39	1.29
GCP 2	X	387181.62	387181.83	-0.20	387182.08	-0.45	387182.54	-0.91
	Y	595667.20	595667.46	-0.26	595667.95	-0.75	595666.02	1.18
GCP 3	X	387227.79	387227.71	0.08	387227.78	0.01	387228.51	-0.72
	Y	595644.78	595644.64	0.14	595645.35	-0.57	595646.34	-1.56
GCP 4	X	387264.95	387265.01	-0.06	387265.09	-0.14	387265.81	-0.86
	Y	595634.08	595633.91	0.16	595634.37	-0.30	595635.10	-1.03
GCP 5	X	387264.52	387264.49	0.02	387265.29	-0.77	387263.82	0.70
	Y	595666.04	595665.89	0.15	595665.07	0.97	595664.22	1.81
GCP 6	X	387221.42	387221.60	-0.18	387222.02	-0.60	387222.39	-0.97
	Y	595699.17	595699.29	-0.12	595700.03	-0.86	595701.06	-1.89

Table 7: Summary of RMSE related to GCPs

RMSE (m)	Reference data	Comparison data	H30	H50	H70
X	GCPs	DSM	0.13	0.50	0.86
Y	GCPs	DSM	0.17	0.74	1.50
		Overall RMSE (m)	0.21	0.89	1.73

Table 8: Errors between actual distance and UAV-derived DSM

Distance measurement error (DSM - Actual)							
Measurement No.	Actual distance (m)	H30 DSM distance (m)	Error (m)	H50 DSM distance (m)	Error (m)	H70 DSM distance (m)	Error (m)
M1	14.10	14.16	0.06	14.19	0.09	13.92	-0.18
M2	5.10	4.95	-0.15	4.96	-0.14	4.75	-0.35
M3	19.65	19.62	-0.03	19.6	-0.05	19.5	-0.15
M4	18.10	17.99	-0.11	17.95	-0.15	17.53	-0.57
M5	15.90	15.8	-0.1	15.6	-0.3	15.5	-0.4
M6	23.05	22.75	-0.3	22.89	-0.16	22.88	-0.17
M7	2.00	2.08	0.08	1.97	-0.03	1.89	-0.11
M8	3.00	2.97	-0.03	3.10	0.1	2.67	-0.33
M9	1.40	1.34	-0.06	1.32	-0.08	1.31	-0.09
M10	1.40	1.34	-0.06	1.33	-0.07	1.32	-0.08

The trend of the real values (horizontal distances) compared to the measured values on the DSM is illustrated in Figure 8. Overall, the data indicates that the modeled values tend to be slightly lower than the actual real-world measurements.

3.4.2 Height measurement error

Table 9 provides a summary of the ten real heights measured on the ground, their corresponding values on each of the Digital Surface Models (DSMs), and the differences between these real values and the estimated values for each mission. The relationship between the real values (heights) and the values measured on the DSM is illustrated in Figure 9. In general, the modeled values tend to be less than or equal to the actual real-world measurements.

3.4.3 Summary of the Results

Across all flight missions, the values obtained from the resulting models are, in most cases, less than or equal to the actual measured values. It has been observed that the horizontal accuracy is superior to the vertical accuracy. This conclusion is drawn from the fact that the estimated and measured values show a better overlap in Figure 8, which illustrates horizontal accuracy, compared to Figure 9, which depicts height accuracy. Table 10 presents a summary of the Root Mean Square Errors (RMSE) associated with the different real measurements taken on the ground. The RMSE for horizontal measurements was found to be 12 cm for mission 1 (H=30m), 14 cm for mission 2 (H=50m), and 29 cm for mission 3 (H=70m). For vertical measurements, the RMSE values were 15 cm for mission 1,27 cm for mission 2, and 58 cm for mission 3.

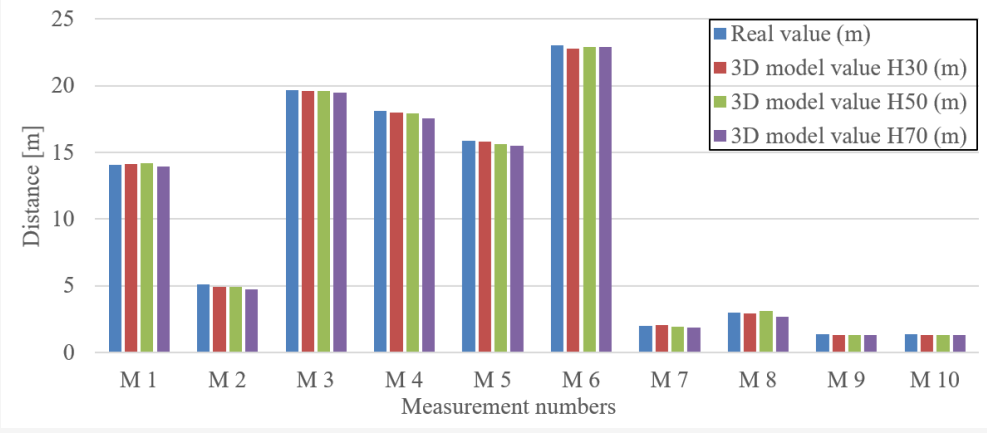

Figure 8: Error in absolute value between actual and model distances bar chart in meter

Table 9: UAV-derived height measurement error

Distance measurement error (DSM - Actual)							
Measurement No.	**Actual distance (m)**	**H30 DSM distance (m)**	**Error (m)**	**H50 DSM distance (m)**	**Error (m)**	**H70 DSM distance(m)**	**Error (m)**
M1	7.30	7.03	-0.27	6.98	-0.32	6.32	-0.98
M2	4.25	4.20	-0.05	3.88	-0.37	4.09	-0.16
M3	4.30	4.33	0.03	4.03	-0.27	3.62	-0.68
M4	4.40	4.16	-0.24	4.21	-0.19	3.75	-0.65
M5	3.07	2.91	-0.16	2.73	-0.34	2.42	-0.65
M6	2.92	2.73	-0.19	2.59	-0.33	2.21	-0.71
M7	3.46	3.34	-0.12	3.20	-0.26	2.80	-0.66
M8	3.46	3.45	-0.01	3.43	-0.03	3.40	-0.06
M9	4.40	4.25	-0.15	4.12	-0.28	4.10	-0.30
M10	4.30	4.24	-0.06	4.20	-0.10	4.00	-0.30

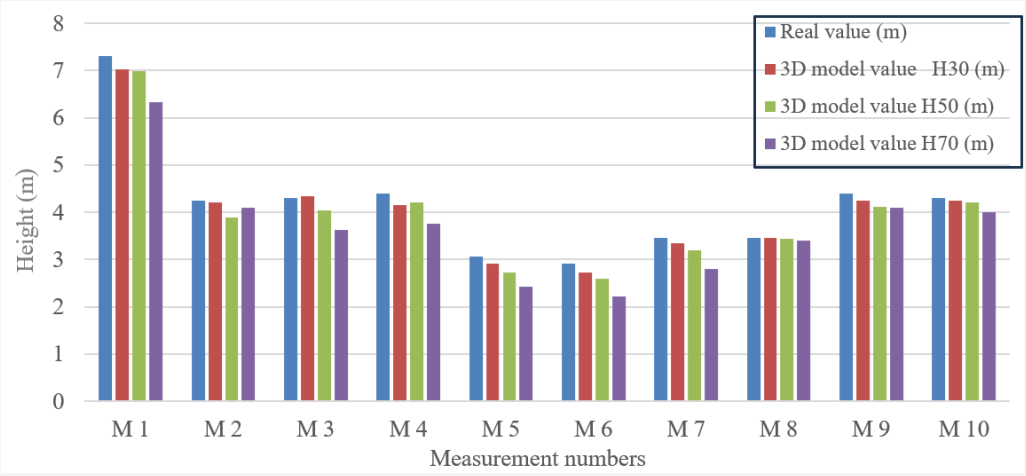

Figure 9: Gap in absolute value between real and model heights bar chart in meter

4. Discussions

The high planimetric accuracy (in the centimeter range) observed for the flight at 30 meters altitude demonstrates the effective rendering quality of the corresponding DSM. The gradual decline in planimetric accuracy with increased flight altitude is attributed to reduced visibility of ground details. As the flight altitude increases, the drone's field of vision encompasses a larger area, but specific details, such as building outlines and sewer grates, begin to blur. The DSM's accuracy in this study is further affected by the presence of vegetation and constructions within the study area, complicating the modeling process with high precision.

Horizontal measurements on the ground exhibit greater accuracy than vertical measurements, as evidenced by the lower RMSE values for horizontal measurements compared to vertical ones across all flight missions. This increased accuracy is due to the clear visibility of these areas (on bare ground) from the drone's elevated position. Any area that is well-photographed and appears in at least five images from a mission is accurately represented in the DSM, with a margin of error reduced to 1 cm; this is illustrated by points 9 and 10 in Table 8. Therefore, obtaining a sufficient number of images is crucial for achieving a more accurate DSM.

Vertical measurements, however, are influenced by the camera's tilt angle. If a building facade is not captured in at least five different images, it is poorly represented in the DSM. Conversely, as the drone flies over the area of interest, it overflies obstacles, ensuring that the heights of structures (such as buildings or trees) are correctly captured. Lower flight altitudes result in higher accuracy, as evidenced by Table 9, where the best RMSE values were obtained during the 30-meter flight mission. This can be attributed to the high quality of images captured at lower altitudes (30 meters in this study), which yields a denser point cloud compared to flights at higher altitudes (70 meters in this study) [17]. The superior image quality contributes to a more precise rendering after photogrammetric processing.

The findings of this study indicate that higher drone altitudes during image capture correlate with decreased DSM accuracy, as demonstrated by the 70-meter flight (mission 3), which achieved a horizontal accuracy of 29 cm and a vertical accuracy of 58 cm, compared to the 30-meter flight, which achieved a horizontal accuracy of 12 cm and a vertical accuracy of 15 cm. To achieve higher accuracy, a greater number of images and lower flight altitudes are necessary; however, this requires longer flight times and limits the area that can be covered in a single mission. The optimal approach is to avoid excessively high altitudes to maintain DSM quality, while also avoiding excessively low altitudes to ensure adequate area coverage within a reasonable flight duration.

In the field of telecommunications, particularly in the study of electromagnetic wave propagation in urban environments, accurately representing the environment primarily involves identifying the location, width, and height of each obstacle (e.g., buildings and trees). The best Digital Elevation Models (DEMs) used in ray-tracing models for telecommunications had an accuracy of 25 meters [18]. These DEMs, which are inadequate for accurately representing the environment, are no longer suitable given the new radio frequencies being used.

The 30-meter flight mission with 12 cm horizontal and 15 cm vertical accuracy, the 50-meter flight mission with 14 cm horizontal and 27 cm vertical accuracy, and the 70-meter flight mission with 29 cm horizontal and 58 cm vertical accuracy in this study demonstrate that it is possible to obtain a DSM with centimeter-level accuracy for modeled structures (buildings and trees). These DSM data can be effectively used in electromagnetic wave propagation models.

5. Conclusion

This study demonstrates that it is feasible to generate a Digital Surface Model (DSM) with a planimetric accuracy of up to 21 cm, a distance accuracy of up to 12 cm, and a height accuracy of up to 15 cm using a DJI Phantom 4 Pro drone for data collection and Pix4Dmapper software for photogrammetry. It is crucial, however, to carefully select the camera angle and drone altitude to ensure the accurate inclusion of building facades in the captured images. The accuracy of a specific area within the DSM is closely aligned with reality when it is well-photographed and appears in at least five different images. For creating a 3D model with textures that closely resemble reality, it is recommended to fly closer to the target and capture a large number of images from various angles. To achieve accurate height measurements of ground elements, a flight altitude of 50 m and a camera tilt angle of 70° are suggested, as demonstrated in this study. The findings confirm that it is possible to produce a DSM with centimeter-level accuracy, which can significantly enhance applications in fields like telecommunications, particularly for studying the propagation of high-frequency electromagnetic waves with greater precision.

References

[1] Ouedraogo, M., Aurore, D. and Charles, D., (2014). Synthèse Bibliographique : le Modèle Numérique de Terrain de Haute Résolution, Ses Erreurs et Leur Propagation. *Biotechnology, Agronomy, Society and Environment*, Vol. 18, 407-421.

[2] Elias, M., Isfort, S., Eltner, A. and Maas, H. G., (2024). UAS Photogrammetry for Precise Digital Elevation Models of Complex Topography: A Strategy Guide. *International Society for Photogrammetry and Remote Sensing*, Vol. X-2-2024. https://doi.org/10.5194/isprs-annals-X-2-2024-57-2024.

[3] Pinatibi H., Coulibaly, N., Coulibaly, T. J. H. and Savané, I., (2016). Characterization of Error on a Digital Elevation Model (DEM) Based on Morphological Zones: Case of the Denguélé District (North-west of Côte d'Ivoire). *International Journal of Innovation and Applied Studies*, Vol. 16, 84–93.

[4] Stephanie, R. R., Ian, M. and William, L., (2020). Comparing the Spatial Accuracy of Digital Surface Models from Four Unoccupied Aerial Systems: Photogrammetry Versus LiDAR. *Remote Sensing*, Vol. 12, 2806-2823. https://doi.org/10.3390/rs12172806.

[5] Long, N., Millescamps, B., Lévêque, F., Lachaussée, N., Pouget, F. and Bertin, X., (2016). *Génération d'un MNT à Partir d'images Acquises par Drone: A Quelle Précision Verticale Peut-On Prétendre ?*. Available: https://www.researchgate.net/publication/299371129_Generation_d'un_MNT_a_partir_d'images_acquises_par_drone_a_quelle_precision_verticale_peut-on_pretendre [Accessed June 05, 2024].

[6] Tomas, U., Tapani, R., Juha, O. and Tapani, S., (2008). Distributed Error Propagation Analysis for Automatic Drainage Basin Delineation. *Proceeding of the 8th International Symposium on Spatial Accuracy Assessment in Natural Resources and Environmental Sciences*, June 25-27, Shanghai, P. R. China, 126-133. Available: https://www.researchgate.net/publication/228948442_Distributed_error_propagation_analysis_for_automatic_drainage_basin_delineation [Accessed June 05, 2024].

[7] Carter, J. R., (1988). Digital Representations of Topographic Surfaces. *Photogrammetric Engineering & Remote Sensing*, Vol. 54, 1577-1580.

[8] Bouziani, M., Amraoui, M. and Kellouch, S., (2021). Comparison Assessment of Digital 3d Models Obtained by Drone Based LIDAR and Drone Imagery. *International Society for Photogrammetry and Remote Sensing*, Vol. XLVI-4/W5-2021. https://doi.org/10.5194/isprs-archives-XLVI-4-W5-2021-113-2021.

[9] Chonpatathip, S., Suanpaga, W., and Chantawarangul, K. (2023). Utilizing Unmanned Aerial Vehicles (UAVs) for Earthwork Fill Height Determination in Road Construction. *International Journal of Geoinformatics*, Vol. 19(10), 28–39. https://doi.org/10.52939/ijg.v19i9.2877.

[10] Natacha, V., Nicolas, L., Thierry, G., Nathalie, L. and Xavier, B., (2021). *Évaluation de la Précision Verticale du Modèle Numérique de Surface à Partir d'images Acquises Avec l'eBee X RTK*. Journées Drones & Capteurs Embarqués 2021, Sep 2021, Saint-Pierre-d'Oléron, France. Available: https://hal.science/hal-03401093v1 [Accessed June 05, 2024].

[11] Gonzalez-Aguilera, D. and Gomez-Lahoz, J., (2009). Forensic Terrestrial Photogrammetry from a Single Image. *Journal of Forensic Sciences*, Vol. 54(6), 1376-1387. https://doi.org/10.1111/j.1556-4029.2009.01170.x.

[12] Nelson, A., Reuter, H. I. and Gessler, P., (2009). DEM Production Methods and Sources. Geomorphometry: Concepts, Software, Applications. *Developments in Soil Science*, Vol. 33, 65-85.

[13] Küng, O., Strecha, C., Beyeler, A., Zufferey, J., Floreano, D., Fua, P. and Gervaix, F., (2011). The Accuracy of Automatic Photogrammetric Techniques on Ultra-Light UAV Imagery. *The International Archives of the Photogrammetry, Remote Sensing and Spatial Information Sciences*, Vol. 38-1(C22), 1-7. https://doi.org/10.5194/isprsarchives-XXXVIII-1-C22-125-2011.

[14] La Côte d'Ivoire: Météo du 26 septembre 2023. historique-meteo.net. Available: https://www.historique-meteo.net/afrique/cote-d-ivoire/2023/09/26/. [Accessed Sept. 03, 2024].

[15] La Côte d'Ivoire: Météo du 27 septembre 2023. historique-meteo.net. Available: https://www.historique-meteo.net/afrique/cote-d-ivoire/2023/09/27/. [Accessed Sept. 03, 2024].

[16] La Côte d'Ivoire: Météo du 02 octobre 2023. historique-meteo.net. Available: https://www.historique-meteo.net/afrique/cote-d-ivoire/2023/10/02/. [Accessed Sept. 03, 2024].

[17] Agüera-Vega, F., Agüera-Puntas, M., Martínez-Carricondo, P., Mancini, F. and Carvajal, F., (2020). Effects of Point Cloud Density, Interpolation Method and Grid Size on Derived Digital Terrain Model Accuracy at Micro Topography Level. *International Journal of Remote Sensing*, Vol. 41(21), 8281-8299. https://doi.org/10.1080/01431161.2020.1771788.

[18] Christine, T., (2005). *Prédiction de Couverture de Champ Radioélectrique Pour Les Réseaux Radiomobiles: L'apport des Systèmes d'Information Géographique. Application en Milieu Urbain*, Géographie. Université Louis Pasteur - Strasbourg I., Français.